molecular pharmaceutics

articles

Quantitative Assessment of the Cell Penetrating Properties of RI-Tat-9: Evidence for a Cell Type-Specific Barrier at the Plasma Membrane of Epithelial Cells

Xiaoping Zhang,[†] Li Wan,[†] Shahriar Pooyan,[†] Yaming Su,[†] Carol R. Gardner,[‡] Michael J. Leibowitz,[§,||] Stanley Stein,[†,||] and Patrick J. Sinko*[,†,||]

Department of Pharmaceutics, Ernest Mario School of Pharmacy, Rutgers University, Piscataway, New Jersey 08854-0789, Environmental and Occupational Health Sciences Institute, Department of Pharmacology and Toxicology, Rutgers University, Piscataway, New Jersey 08854, Department of Molecular Genetics, Microbiology, and Immunology, Robert Wood Johnson Medical School, University of Medicine and Dentistry of New Jersey, Piscataway, New Jersey 08854, and Cancer Institute of New Jersey, New Brunswick, New Jersey 08903-2681

Received September 27, 2003

Abstract: Penetration of epithelial cells represents the rate-determining step for the absorption of many drugs and pharmaceutical macromolecules such as proteins and nucleic acid therapeutics. While the potential of using cell-penetrating peptides (CPPs) to facilitate absorption has been increasingly recognized, the mechanism of cell penetration and the uptake into certain cells have recently been called into question due to methodological artifacts. Therefore, the objective of this study was to quantitatively assess the ability of RI-Tat-9, a proteolytically stable CPP, to penetrate epithelial cell monolayers. The permeability of RI-Tat-9 with two epithelial cell lines, Madin-Darby canine kidney (MDCK) and Caco-2 cells, was comparable to the leakiness of the respective intact monolayers. Microscopic imaging showed that fluorescence-tagged RI-Tat-9 did not enter these cells, further supporting a paracellular transport mechanism. Although insufficient data were generated in these studies to generalize the observed phenomenon, the entry of RI-Tat-9 into nonepithelial T lymphocytic MT2 cells, possibly by endocytosis, suggested that a cell type-specific barrier might exist that controlled uptake of RI-Tat-9 by cells. Compared to that in MT2 and HeLa cells, the active uptake of the peptide into MDCK monolayers was much slower and showed no dependence of cell energy. Furthermore, the equilibrium binding of RI-Tat-9 to MDCK cells at 0 °C was indicative of an interaction with a nonspecific receptor. A correlation between binding density and concentration difference across a leaky separation barrier suggested that repulsion of free peptide molecules by bound peptide molecules at the MDCK monolayer surface may be significant at micromolar concentrations. The results of this study quantitatively show that Tat CPP uptake into two commonly used epithelial cell types is minimal and possibly cell type-specific. Implications for Tat CPP-assisted drug delivery are discussed.

Keywords: HIV-1 Tat peptide; cell-penetrating peptide; CPP-assisted drug delivery; protein transduction domain

Introduction

Cell-penetrating peptides (CPPs), also known as protein transduction domains (PTDs), are a collection of different families of short peptides believed to enter cells by penetrating cell membranes in a cell type- and cell energy-independent manner.[1−4] These families include peptides derived from several cell-penetrating proteins (e.g., transcriptional activators and anti-DNA antibodies), signal

* To whom correspondence should be addressed. Telephone: (732) 445-3831, ext. 213. Fax: (732) 445-4271. E-mail: sinko@rci.rutgers.edu.

† Ernest Mario School of Pharmacy, Rutgers University.

‡ Department of Pharmacology and Toxicology, Rutgers University.

§ University of Medicine and Dentistry of New Jersey.

|| Cancer Institute of New Jersey.

10.1021/mp034014y CCC: $27.50
Published on Web 01/28/2004

sequence-based peptides, hydrophobic membrane translocating sequence peptides, and designed peptides. Examples of such transcriptional activators are the HIV-1 Tat protein, HSV-1 VP22 protein, and fruit fly Antennapedia homeodomain. CPPs have attracted a considerable amount of interest, and hopes of using CPPs for enhancing gene therapy, vaccine development, and drug delivery have been raised.[5,6]

The widely used Tat CPPs are derived from the HIV-1 Tat protein. Deletion studies have identified a region in the protein responsible for cell penetration: a nine-residue, highly positively charged basic domain (RKKRRQRRR, Tat_{49-57}).[7−9] So far, the use of at least 10 Tat-derived CPPs containing this domain has been reported. Mutagenesis studies have demonstrated that the critical feature of the basic domain is the guanidinium group of the arginine residues and the positive charge; other factors, such as sequence, a potential nuclear localization signal within the domain, chirality, or the linear configuration, are not essential.[9−11] In fact, the L- or D-form of eight- or nine-residue polyarginine is at least as efficient as the L-form Tat_{49-57} in cell penetration,[9−11] as is the retro−inverso form (RI-form) of Tat_{48-57}.[12] The Tat protein functions mainly as a transcriptional activator of HIV-1 virus. It binds to the TAR structure in the 5′-region of all HIV-1 transcripts.[13,14] Remarkably, the TAR-binding region in the Tat protein has been mapped to virtually the same region (Tat_{48-59}) as that identified for cell penetration (Tat_{49-57}), and again, the important feature is arginine within the RRXRR stretch.[13−15] Since the Tat protein is essential for HIV-1 replication, disruption of the interaction between Tat and TAR is a viable strategy for combating HIV infection. We have demonstrated that an L-form of a Tat CPP and an L-form Tat CPP conjugate[16,17] as well as an RI-form of a Tat CPP, named RI-Tat-9 (RI-CK-Tat_{57-49}) (L. Wan, unpublished results), have potent anti-HIV activity *in vitro*. Unlike the case in many other CPPs, the anti-HIV activity demonstrates cell entry by a Tat CPP alone without the complication of carrying a bulky cargo.

Despite intense study, the exact cell penetration mechanism of any of the CPPs remains unknown.[1−4,11] Two different mechanistic models have been proposed,[18,19] but not experimentally substantiated. The unusual and useful ability of Tat CPPs to apparently enter cells regardless of cell type and independent of temperature distinguishes Tat CPPs from non-cell-penetrating peptides. In addition, the Tat protein, which can be viewed as a Tat CPP fused to a small protein, is able to cross cell plasma membranes in both directions.[20] These mechanistic features of Tat CPPs underlie all studies aimed at Tat CPP-assisted drug delivery. That is, Tat CPPs are believed to penetrate not only a layer of the plasma membrane but also layers of cells.

Tat CPP-assisted cargo delivery has been reported in a variety of experimental protocols.[1−6] *In vitro*, Tat CPPs have been shown to ferry various cargos (e.g., nucleic acids,

(1) *Cell-penetrating peptides: processes and applications*; Langel, U., Ed.; CRC Press: Boca Raton, FL, 2002.
(2) Fischer, P. M.; Krauz, E.; Lane, D. P. Cellular delivery of impermeable effector molecules in the form of conjugates with peptides capable of mediating membrane translocation. *Bioconjugate Chem.* **2001**, *12*, 825−841.
(3) Hawiger, J. Noninvasive intracellular delivery of functional peptides and proteins. *Curr. Opin. Chem. Biol.* **1999**, *3*, 89−94.
(4) Lindgren, M.; Hallbrink, M.; Prochiantz, A.; Langel, U. Cell-penetrating peptides. *Trends Pharmacol. Sci.* **2000**, *21*, 99−103.
(5) Morris, M. C.; Chaloin, L.; Heitz, F.; Divita, G. Translocating peptides and proteins and their use for gene delivery. *Curr. Opin. Biotechnol.* **2000**, *11*, 461−466.
(6) Wadia, J. S.; Dowdy, S. F. Modulation of cellular function by TAT mediated transduction of full length proteins. *Curr. Protein Pept. Sci*. **2003**, *4*, 97−104.
(7) Fawell, S.; Seery, J.; Daikh, Y.; Moore, C.; Chen, L.; Pepinsky, B.; Barsoum, J. Tat-mediated delivery of heterologous proteins into cells. *Proc. Natl. Acad. Sci. U.S.A.* **1994**, *91*, 664−668.
(8) Vives, E.; Brodin, P.; Lebleu, B. A truncated HIV-1 Tat protein basic domain rapidly translocates through the plasma membrane and accumulates in the cell nucleus. *J. Biol. Chem.* **1997**, *272*, 16010−16017.
(9) Park, J.; Ryu, J.; Kim, K.; Lee, H. J.; Bahn, J. H.; Han, K.; Choi, E. Y.; Lee, K. S.; Kwon, H. Y.; Choi, S. Y. Mutational analysis of a human immunodeficiency virus type 1 Tat protein transduction domain which is required for delivery of an exogenous protein into mammalian cells. *J. Gen. Virol.* **2002**, *83*, 1173−1181.
(10) Wender, P. A.; Mitchell, D. J.; Pattabiraman, K.; Pelkey, E.; Steinman, L.; Rothbard, J. The design, synthesis, and evaluation of molecules that enable or enhance cellular uptake: peptoid molecular transporters. *Proc. Natl. Acad. Sci. U.S.A.* **2000**, *97*, 13003−13008.
(11) Futaki, S. Arginine-rich peptides: potential for intracellular delivery of macromolecules and the mystery of the translocation mechanisms. *Int. J. Pharm.* **2002**, *245*, 1−7.
(12) Bonny, C.; Oberson, A.; Negri, S.; Sauser, C.; Schorderet, D. F. Cell-permeable peptide inhibitors of JNK: novel blockers of beta-cell death. *Diabetes* **2001**, *50*, 77−82.
(13) Rana, T. M.; Jeang, K. Biochemical and functional interactions between HIV-1 Tat protein and TAR RNA. *Arch. Biochem. Biophys.* **1999**, *365*, 175−185.
(14) Jones, K. A.; Peterlin, B. M. Control of RNA initiation and elongation at the HIV-1 promoter. *Annu. Rev. Biochem.* **1994**, *63*, 717−743.
(15) Green, M.; Loewenstein, P. M. Autonomous functional domains of chemically synthesized human immunodeficiency virus Tat Trans-activator protein. *Cell* **1998**, *55*, 1179−1188.
(16) Choudhury, I.; Wang, J.; Rabson, A. B.; Stein, S.; Pooyan, S.; Stein, S.; Leibowitz, M. J. Inhibition of HIV-1 replication by a Tat RNA-binding domain peptide analog. *J. Acquired Immune Defic. Syndr. Hum. Retrovirol*. **1998**, *17*, 104−111.
(17) Huang, S.; Pooyan, S.; Wang, J.; Choudhury, I.; Leibowitz, M. J.; Stein, S. A polyethylene glycol copolymer for carrying and releasing multiple copies of cysteine-containing peptides. *Bioconjugate Chem.* **1998**, *9*, 612−617.
(18) Derossi, D.; Calvet, S.; Trembleau, A.; Brunissen, A.; Chassaing, G.; Prochiantz, A. Cell internalization of the third helix of the Antennapedia homeodomain is receptor-independent. *J. Biol. Chem.* **1996**, *271*, 18188−18193.
(19) Hallbrink, M.; Floren, A.; Elmquist, A.; Pooga, M.; Bartfai, T.; Langel, U. Cargo delivery kinetics of cell-penetrating peptides. *Biochim. Biophys. Acta* **2001**, *1515*, 101−109.
(20) Chang, H.; Samaniego, F.; Nair, B. C.; Ensoli, B. HIV-1 Tat protein exits from cells via a leaderless secretory pathway and binds to extracellular matrix-associated heparan sulfate proteoglycans through its basic region. *AIDS* **1997**, *11*, 1421−1431.

microspheres, liposomes, polymers, fusion proteins, imaging agents, etc.) into cells, as measured by using microscopy, flow cytometry, agent uptake, and cell functionality. Early *in vivo* work showed that Tat CPPs could deliver various cargos into tissues and organs, including the brain.[1−6,21] However, more recent *in vivo* work has raised questions. While there are some examples of successful delivery,[6] some others are disappointing. A Tat CPP carrying an imaging agent injected into the tail vein was rapidly cleared from mice.[22] When the same conjugate was introduced into rat urinary bladder, no penetration beyond the bladder was seen.[23] Doxorubicin-loaded and Tat CPP-coated liposomes showed neither cytotoxicity *in vitro* nor tumor control in mice.[24] In a mouse model, a conjugate of a Tat CPP bound to an antibody was not able to cross endothelia of tumor blood vessels.[25] A pharmacokinetic study of the CPP_{48-58}−biotin conjugate revealed rapid clearance in rats and no enhancement of bioavailability of streptavidin when bound to the CPP_{48-58}−biotin conjugate.[26] Tat CPP used in conjugates did not change the usual distribution pattern of the cargo macromolecules that was heavily skewed toward organs of the reticulo-endothelial system or the organs of waste elimination.[7,22,26] These observations demonstrate a clear lack of *in vitro*−*in vivo* correlation and imply that either the cell penetration mechanism is more complex than has been suggested or additional factors control the process *in vivo*.

Recently, *in vitro* evidence against the cell penetration mechanism has emerged. It was found that a Tat CPP carrying a hydrophilic imaging agent[23] or a fluorescence tag[27] was localized at the surface of MDCK epithelial monolayers, not inside cells. A Tat CPP−diphtheria toxin A fragment (dtA) fusion protein and another CPP−dtA fusion (VP22−dtA) avidly bound to the cell surface but failed to show detectable cytotoxicity.[28] An explanation for the observed inability of Tat CPP to deliver cargos into cells was provided by the discovery that cell fixation, a common procedure in microscopy, caused two small cell-penetrating proteins, VP22 and histone H1,[29] as well as oligonucleotides[30] to cross cell membranes. There was no cell penetration of a Tat CPP fusion protein unless cell fixation was used.[31] Three groups from three countries jointly published a paper, demonstrating that cell fixation led to artifactual uptake of Tat_{48-60} and $(Arg)_9$.[32] A number of authors[27,31−33] pointed out that this artifact and the lack of a distinction between cell surface binding and internalization were the basis of most of the previous evidence for cell penetration. As a result, some have called for a reevaluation of the cell penetration mechanism[32] or rejection of the term "protein transduction domain".[31] It should be pointed out that these recent reports do not dispute the entry of Tat CPP per se or the validity of Tat CPP-assisted cargo delivery that is based on the cargo's functionality, since some of these reports did show that Tat CPPs, Tat CPP-bound cargo, and $(Arg)_9$ entered some cells in a manner consistent with endocytosis.[32−34]

In this study, a well-controlled quantitative assessment of the cell penetrating ability of a Tat CPP in two commonly used epithelial cell models is presented. The data demonstrate a predominant paracellular transport mode through the epithelial monolayers and do not support the cell type- and cell energy-independent cell penetration mechanism. The data also suggest the existence and relevance of a novel secondary repulsion mechanism.

(21) Schwarze, S. R.; Ho, A.; Vocero-Akbani, A.; Dowdy, S. F. In vivo protein transduction: delivery of a biologically active protein into the mouse. *Science* **1999**, *285*, 1569−1572.

(22) Polyakov, V.; Sharma, V.; Dahlheimer, J. L.; Pica, C. M.; Luker, G. D.; Piwnica-Worms, D. Novel Tat-peptide chelates for direct transduction of technetium-99m and rhenium into human cells for imaging and radiotherapy. *Bioconjugate Chem.* **2000**, *11*, 762−771.

(23) Violini, S.; Sharma, V.; Prior, J. L.; Dyszlewski, M.; Piwnica-Worms, D. Evidence for a plasma membrane-mediated permeability barrier to Tat basic domain in well-differentiated epithelial cells: lack of correlation with heparan sulfate. *Biochemistry* **2002**, *41*, 12652−12661.

(24) Tseng, Y.; Liu, J.; Hong, R. Translocation of liposome into cancer cells by cell-penetrating peptides penetratin and Tat: a kinetic and efficacy study. *Mol. Pharmacol.* **2002**, *62*, 864−872.

(25) Niesner, U.; Halin, C.; Lozzi, L.; Gunthert, M.; Neri, P.; Wunderli-Allenspach, H.; Zardi, L.; Neri, D. Quantitation of the tumor-targeting properties of antibody fragments conjugated to cell-penetrating HIV-1 TAT peptides. *Bioconjugate Chem.* **2002**, *13*, 729−736.

(26) Lee, H. J.; Pardridge, W. M. Pharmacokinetics and delivery of Tat and Tat-protein conjugates to tissues in vivo. *Bioconjugate Chem.* **2001**, *12*, 995−999.

(27) Kramer, S. D.; Wunderli-Allenspach, H. No entry for TAT(44−47) into liposomes and intact MDCK cells: novel approach to study membrane permeation of cell-penetrating peptides. *Biochim. Biophys. Acta* **2003**, *1609*, 161−169.

(28) Falnes, P.; Wesche, J.; Olsnes, S. Ability of the Tat basic domain and VP22 to mediate cell binding, but not membrane translocation of the diphtheria toxin A-fragment. *Biochemistry* **2001**, *40*, 4349−4358.

(29) Lundberg, M.; Johansson, M. Positively charged DNA-binding proteins cause apparent cell membrane translocation. *Biochem. Biophys. Res. Commun.* **2002**, *291*, 367−371.

(30) Pichon, C.; Monsigny, M.; Roche, A. C. Intracellular localization of oligonucleotides: influence of fixative protocols. *Antisense Nucleic Acid Drug Dev.* **1999**, *9*, 89−93.

(31) Leifert, J. A.; Harkins, S.; Whitton, J. L. Full-length proteins attached to the HIV tat protein transduction domain are neither transduced between cells, nor exhibit enhanced immunogenicity. *Gene Ther.* **2002**, *9*, 1422−1428.

(32) Richard, J. P.; Melikov, K.; Vives, E.; Ramos, C.; Verbeure, B.; Gait, M. J.; Chernomordik, L. V.; Lebleu, B. Cell-penetrating peptides. A reevaluation of the mechanism of cellular uptake. *J. Biol. Chem.* **2003**, *278*, 585−590.

(33) Vives, E.; Richard, J. P.; Rispal, C.; Lebleu, B. TAT peptide internalization: seeking the mechanism of entry. *Curr. Protein Pept. Sci.* **2003**, *4*, 125−132.

(34) Console, S.; Marty, C.; Garcia-Echeverria, C.; Schwendener, R.; Ballmer-Hofer, K. Antennapedia and HIV transactivator of transcription (TAT) protein transduction domains promote endocytosis of high molecular weight cargo upon binding to cell surface glycosaminoglycans. *J. Biol. Chem.* **2003**, *278*, 35109−35114.

Materials and Methods

Materials. Sigmacote, protamine, Hoechst 33258, digitonin, HEPES [*N*-(2-hydroxyethyl)piperazine-*N*′-4-butanesulfonic acid], 2-deoxyglucose, and sodium azide were purchased from Sigma (St. Louis, MO), [^{3}H]acetic anhydride and [^{14}C]mannitol from Amersham (Piscataway, NJ), Transwell inserts from Corning/Costar (Acton, MA), Lab-Tek II chamber slides from Nalge Nunc International Corp. (Naperville, IL), siliconized microtubes from Fisher Scientific (Pittsburgh, PA), and tissue culture reagents from Invitrogen/Gibco (Carlsbad, CA). GF120908 was a gift from Dr. J. W. Polli at Glaxo Wellcome, Inc. (Research Triangle Park, NC), and MK561 was a gift from Dr. Koch at Merck & Co., Inc. (Rahway, NJ). All other chemicals and supplies were commercially available.

Peptide Synthesis and Labeling. The RI-Tat-9 peptide in the RI-form (dCdK-dRdRdRdQdRdRdKdKdR or RI-CK-Tat$_{57-49}$) was manually synthesized on MBHA Rink Amide resin via Fmoc chemistry using reagents from NovaBiochem (Laufelfingen, Switzerland). The two additional residues at the N-terminus, Cys and Lys, were reserved for future conjugation and labeling. After cleavage from the solid support and ether precipitation, the peptide was purified by HPLC on a Vydac reverse phase C-18 column and characterized by matrix-assisted laser desorption ionization time-of-flight mass spectrometry. For radiolabeling, the assembled peptide on the solid support (prior to N-acetylation) was allowed to react with tritiated acetic anhydride in the presence of coupling activation reagents BOP [benzotriazol-1-yloxy-tris(dimethylamino)phosphonium hexafluorophosphate], HOBT (1-hydroxybenzotriazole), and DIEA (diisopropylethylamine). Acetylation of the peptide was driven to completion with an excess of unlabeled acetic anhydride. After cleavage from the solid support and ether precipitation, the tritiated RI-Tat-9 was purified essentially the same way as the nonradioactive RI-Tat-9 by HPLC on a Vydac reverse phase C-18 column and was monitored with a β-RAM flow-through monitor from IN/US Systems (Tampa, FL). For FITC (fluorescein isothiocyanate) labeling of RI-Tat-9, the assembled peptide on the solid support (prior to N-acetylation) was deprotected using the ϵ-NH_2 group of the N-terminal Lys. The exposed NH_2 group was then reacted with NHS (*N*-hydroxysuccinimide)-bound FITC from Sigma, resulting in FITC-bound RI-Tat-9. The purification and characterization of the peptide after FITC labeling were the same as those for the nonradioactive RI-Tat-9.

Cells and Cell Culture. Caco-2, MDCK (Madin-Darby canine kidney), and HeLa cells were purchased from American Type Culture Collection (Rockville, MD). MT2 cells were obtained from D. Richman through the AIDS Research and Reference Reagent Program (Division of AIDS, National Institute of Allergy and Infectious Diseases, National Institutes of Health, Bethesda, MD). Cell culture conditions were the same as reported in refs 35 and 36 except that MT2 cells used RPMI 1640 medium and HeLa cells used Eagle's minimum essential medium.

Determination of the Permeability of MDCK and Caco-2 Monolayers. Directional transport across Caco-2 and MDCK monolayers grown on Transwell inserts (polycarbonate) was performed as described previously[36] with a modification in sampling time (every 30 min for 3 h). The effective permeability (P_e) was calculated using the following equation:

$$P_e = (dC/dt)(V/C_0A)$$

where dC/dt is the permeability rate (the slope of a plot of receiver side concentration over time), V is the buffer volume of a receiver side well, C_0 is the initial RI-Tat-9 concentration applied to the donor side, and A is the surface area of an insert membrane. The wells of one or more 12-well plates were wiped with Sigmacote the day before the experiment to minimize the adsorption of tritiated RI-Tat-9 to the receiver side walls. The coated plates were left in a chemical hood overnight to dry. On the day of the experiment, the coated wells were washed three times with sterile buffer. The Transwell inserts with monolayers growing on them were briefly washed with warm buffer and transferred to the Sigmacote-precoated wells before the incubation with buffers or medium containing tritiated RI-Tat-9 was started. The paracellular permeability of monolayers during culture was monitored by TEER (transepithelial electrical resistance) and during the measurement of P_e by using the paracellular marker mannitol.

Fluorescence and Confocal Microscopy. No cell fixation was used. MDCK and Caco-2 monolayers grown on chamber slides were used 2 and 14 days postconfluency, respectively. MT2 cells were used during exponential growth in suspension. Before being stained, all cells were washed briefly with warm medium without serum. MDCK and Caco-2 monolayers were then live stained in chambers and MT2 cells in siliconized microtubes with 10 μM FITC−RI-Tat-9 conjugate and 2 μM Hoechst 33258 in serum-free medium for 60 min in a 5% CO_2 incubator at 37 °C and washed once with warm Hank's buffered saline (Hank's), followed by staining with a trypan blue solution (Invitrogen/Gibco) at room temperature for 2 min and two washes with Hank's. Trypan blue (excitation at 543 nm and emission at >590 nm) marks dead cells and quenches FITC fluorescence in these cells. Hoechst 33258 is a membrane-permeable live DNA dye. Prepermeation with digitonin (25 μg/mL in serum-free medium) was carried out for MDCK and Caco-2 monolayers at 37 °C for 30 min with one time wash afterward. During the staining,

(35) Luo, F.; Paranjpe, P. V.; Guo, A.; Rubin, E.; Sinko, P. J. Intestinal transport of irinotecan in Caco-2 and MDCK II cells overexpressing efflux transporters Pgp, cMOAT, and MRP1. *Drug Metab. Dispos*. **2002**, *30*, 763−770.

(36) Guo, A.; Marinaro, W.; Hu, P.; Sinko, P. J. Delineating the contribution of secretory transporters in the efflux of etoposide using Madin-Darby canine kidney (MDCK) cells overexpressing P-glycoprotein (Pgp), multidrug resistance-associated protein (MRP1), and canalicular multispecific organic anion transporter (cMOAT). *Drug Metab. Dispos*. **2002**, *30*, 457−463.

the lids of MT2 tubes were open and the tubes were periodically flicked to resuspend cells. Solution exchange during the wash of MT2 cells was achieved by centrifugation at 400*g* for 2 min and gentle cell resuspension with a pipet. The stained monolayers on slides (with chambers removed) and MT2 cells placed on slides were covered with coverslips. The slides were then observed under a Zeiss Axiostar Plus fluorescence microscope with an objective magnification of 63× and an Insight digital camera (in place of eyepieces) with proper filter sets. Digital images were taken with the Insight digital camera and its companion Spot software. Confocal imaging of MT2 cells was performed on a Meridian 570 Anchored Cell Analysis System at the Environmental and Occupational Health Science Institute/Cancer Institute of New Jersey Core Flow Cytometry facility.

Measurement of the Amount of Cell-Associated RI-Tat-9. MDCK monolayers grown on 24-well plates for 2 days postconfluency or aliquots of 2×10^6 MT2 cells in siliconized microtubes were washed briefly, followed by incubation with uptake buffer [0.25 mL per well or per tube of the indicated concentration of tritiated RI-Tat-9 in Hank's and 20 mM HEPES (pH 7.4)] at the indicated temperatures for the indicated times. The 0 °C incubation was achieved by placing plates or microtubes on ice. The wells or tubes were then washed once with 1.2 mL/well or 0.6 mL/tube of Hank's at the indicated temperatures. Aliquots of 0.25 mL of acid wash solution [0.5 M sodium chloride and 0.2 M acetic acid (pH 2.5)] at room temperature were added to acid wash wells or tubes and aliquots of 0.25 mL of Hank's to controls. After 5 min on ice, all wells or tubes were washed twice with 1.2 mL/well or 0.6 mL/tube of ice-cold Hank's. Cells were lysed with 150 μL of 1 N NaOH overnight and neutralized with 150 μL of 1 N HCl the next day. The radioactivity in 260 μL of each lysate was measured by liquid scintillation counting, which was normalized against the cell protein amount as determined with 25 μL of each lysate using the protein assay reagent from Bio-Rad (Hercules, CA). For cell energy starvation experiments, MDCK monolayers and MT2 cells were pretreated with 1 and 0.5% sodium azide in serum-free medium for 30 and 20 min, respectively, followed by incubation with uptake medium containing a 10-fold excess of 2-deoxyglucose to glucose. The uptake procedure of cell energy starvation was the same as that of nonstarved experiments except that tissue culture medium without serum replaced Hank's to improve the viability of MT2 cells. The uptake under starvation conditions was carried out in a 5% CO_2 incubator. Trypan blue staining was used in all procedures to monitor cell viability. To rule out a possible hypertonicity effect of the acid wash [0.5 M sodium chloride and 0.2 M acetic acid (pH 2.5)], 1.25 M sucrose was used as a control, and no significant effect on cell association was found with both types of cells (data not shown).

Curve Fitting. Curve fitting by nonlinear regression used the equation of one-site binding [$Y = (B_{max}X)/(K_d + X)$] with the aid of Prizm 3.03 from GraphPad Software (San Diego, CA), where Y and X were the values of each data point on the two axes.

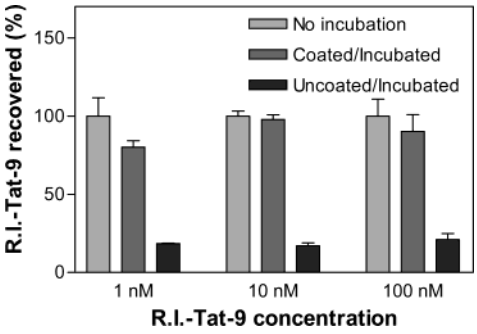

Figure 1. Effect of precoating on reduction of adsorption. Wells of 12-well plates were wiped with Sigmacote, air-dried, and then preincubated overnight with 1.5 mL of 1.5% protamine in water per well. After the wash, tritiated RI-Tat-9 (0.5 mL/well) at 1, 10, and 100 nM in Hank's was added to the precoated wells and the uncoated wells. The plates were incubated at 37 °C for 6 h, and the radioactivities of the contents of all wells were determined by liquid scintillation. The radioactive incubation buffers prior to incubation were also counted and shown as No incubation. Values are means of triplicate determinations ± the standard deviation.

Table 1. Mass Balance of RI-Tat-9 after an A to B Transport Experiment (MDCK Monolayers)

[RI-Tat-9] (μM)	donor (%)	monolayer/insert (%)	receiver (%)	sum (%)[a]
1	66.7 ± 1.9	8.2 ± 0.1	2.0 ± 0.3	76.9 ± 2.3
10	77.1 ± 1.9	5.6 ± 0.1	1.7 ± 0.1	84.4 ± 2.1
100	86.3 ± 2.0	2.2 ± 0.1	3.0 ± 0.2	91.5 ± 2.3

[a] At the end of this 3 h A to B transport experiment, the radioactivities of the donor side buffer (donor), the monlolayer/insert, and the receiver side buffer (receiver) were counted and expressed as a percentage of that applied to give the sum. The receiver wells were precoated with Sigmacote. Values are means of triplicate determinations ± the standard deviation.

Molecular Modeling. A three-dimensional structure of a RI-Tat-9 molecule was constructed and analyzed using ChemBats3D Ultra 7.0 (www.CambrigeSoft.com). Steric and charge energy minimization was employed during the model building. The size of the modeled RI-Tat-9 molecule is represented by the distances of three pairs of atoms that are most distantly separated in the *x*, *y*, and *z* dimensions.

Results

Minimization of Adsorption of RI-Tat-9 to Plastic Surfaces. Preliminary experiments showed that adsorption of RI-Tat-9 to plastic surfaces resulted in a mass balance (recovery) of merely 30% at the end of an apical (A) to basolateral (B) transport experiment. As a result, the transported amount could not be accurately determined. Precoating with Sigmacote and protamine was highly effective in reducing the adsorption at concentrations relevant to this study (Figure 1). Since Sigmacote precoating alone was later found to be equally effective, this pretreatment was used in all reported transport experiments. A mass balance of ≥75% was typically achieved (Table 1).

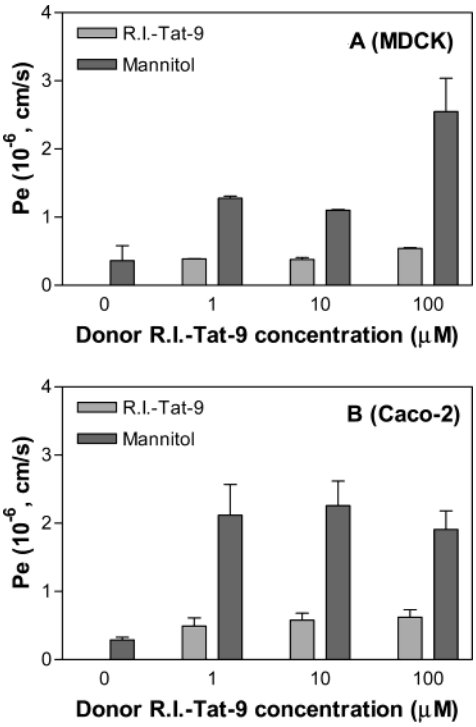

Figure 2. Permeability in the A to B direction through MDCK and Caco-2 monolayers. MDCK or Caco-2 monolayers were grown on polycarbonate Transwell inserts. The donor side incubation buffer contained tritiated RI-Tat-9 at the indicated concentrations and mannitol at a constant concentration of 1 μM. The receiver wells were precoated with Sigmacote. Values are means of triplicate determinations $\pm$ the standard deviation.

Determination of the Permeability of MDCK and Caco-2 Monolayers. These two cell lines and tritiated RI-Tat-9 were used to quantitatively determine the effective permeability (P_e). P_e is based on the measurement of the permeation rate at steady state over several time points and normalized for the donor side concentration. It permits the comparison of permeability at different concentrations.

The ability of tritiated RI-Tat-9 to cross MDCK and Caco-2 monolayers was minimal (<3%; cf. Table 1) in repeated experiments, while the percentage of recovery at the receiver side of empty Transwell inserts was greater than 95% at all three tested concentrations [1, 10, and 100 μM (data not shown)]. These concentrations were chosen because they spanned the noncytotoxic concentration range of Tat CPPs (refs 1 and 11 and our unpublished data). Panels A (MDCK) and B (Caco-2) of Figure 2 show that, at these concentrations, the A to B P_e of RI-Tat-9 was comparable to that of mannitol (control, i.e., RI-Tat-9 concentration of 0), a commonly used marker of paracellular permeability. Mannitol permeability increased moderately but significantly in the presence of RI-Tat-9. This could be one possible mechanism for limited enhancement of tissue penetration by Tat CPPs. The B to A MDCK P_e values of RI-Tat-9 were comparable to the A to B permeabilities for these three concentrations [(0.54 ± 0.12), (0.48 ± 0.07), and $(0.81 \pm 0.07) \times 10^{-6}$ cm/s, respectively]. Therefore, the permeability of RI-Tat-9 with these two types of epithelial monolayers is comparable to the leakiness of their intact tight junctions, which is contrary to what would be expected from the cell penetrating mechanism. The P_e of RI-Tat-9 stays relatively constant in both directions as the concentration varies from 1 to 100 μM, indicating it is not saturable over that concentration range. The nonsaturability suggests that the RI-Tat-9 crosses the epithelial monolayers by passive diffusion.

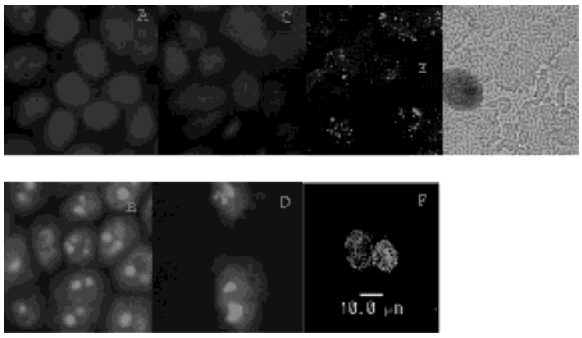

Figure 3. Fluorescence and confocal microscopic images of MDCK and Caco-2 monolayers and suspended MT2 cells. Shown are merged FITC and Hoechst 33258 images of nonpermeated monolayers [(A) MDCK and (C) Caco-2], FITC images only of permeated monolayers [(B) MDCK and (D) Caco-2], FITC image (E), and transmitted light image (G) of the same field of nonpermeated MT2 cells, and confocal FITC image of MT2 cells (F, a middle cell slice). Note a dead cell in G is stained with trypan blue, and the cell's otherwise intense FITC fluorescence has been quenched by trypan blue in panel E. Images of panels A−E and G were taken with a 63× objective lens and an Insight digital camera, whereas the cell size in panel F is referenced to the scale bar.

Fluorescence and Confocal Microscopy. Given the low transmonolayer permeability (Figure 2A,B) of RI-Tat-9, microscopy was used to determine if the predominant mechanism of transport was transcellular or paracellular. Lymphocytic MT2 cells were used as a nonepithelial control since RI-Tat-9 exhibited anti-HIV-1 activity in infected MT2 cells, suggesting sufficient cellular uptake of the peptide (L. Wan, unpublished results). Figure 3 shows fluorescence and confocal microscopy images of MDCK and Caco-2 monolayers and suspended MT2 cells. In Figure 3A, the nuclei of a MDCK monolayer are stained with Hoechst 33258, but no appreciable FITC fluorescence is seen in this two fluorescence-merged image, which indicates that MDCK cells are permeable to Hoechst 33258, but not to the FITC−RI-Tat-9 conjugate. However, when the plasma membrane was pretreated with a mild detergent, digitonin, bright FITC fluorescence of nuclei (especially, nucleoli) and, to a lesser extent, cytosol is seen (Figure 3B). Similar findings are shown in panels C and D of Figure 3 for Caco-2 monolayers. In contrast to these monolayers, in nonpermeated MT2 cells there is a punctate FITC fluorescence distribution (Figure 3E), indicative of endocytosis. No autofluorescence was seen with unstained MT2 cells (images not shown). Confocal

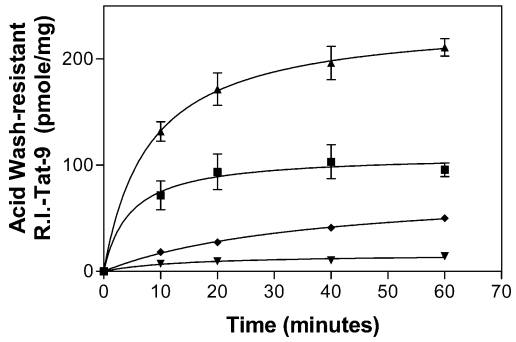

Figure 4. Association of tritiated RI-Tat-9 with MDCK monolayers and MT2 cells: (▲) MT2 at 37 °C, (■) MT2 at 0 °C, (◆) MDCK at 37 °C, and (▼) MDCK at 0 °C. Values are means of triplicate determinations ± the standard deviation. The R^2 of curve fitting by nonlinear regression was greater than 0.964.

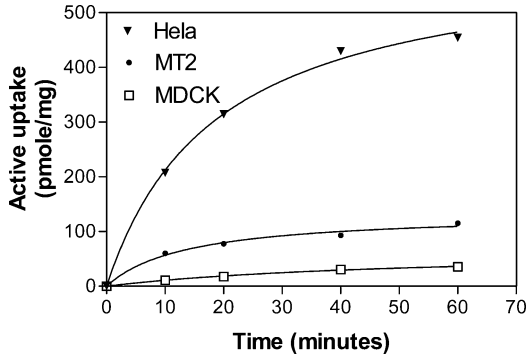

Figure 5. Active uptake of tritiated RI-Tat-9 into HeLa and MT2 cells and MDCK monolayers. The difference in cellular association between 0 and 37 °C in Figure 4 is taken to be active uptake and replotted in Figure 5. The HeLa cell line is added since HeLa cells do not have a high percentage of dead cells as MT2 cells do: (▼) HeLa, (●) MT2, and (□) MDCK.

microscopic images (Figure 3F) indicate that the fluorescence is inside MT2 cells. The microscopy data indicate that FITC−RI-Tat-9 monolayer penetration occurs paracellularly in MDCK and Caco-2 cells, while MT2 cell uptake was significant and was likely to occur by endocytosis. In an attempt to explain a possible mechanism for this phenomenon, MDCK monolayers were exclusively used in subsequent experiments because of their faster monolayer maturation and weaker tendency to form foci.

Measurement of the Amount of Cell-Associated RI-Tat-9. To understand why RI-Tat-9 was unable to enter epithelial monolayers, the time, physiological temperature, cell energy, and concentration dependence of the association of the peptide with MDCK monolayers were quantitatively studied, using MT2 cells as a nonepithelial control. These experiments were performed to address two issues: (1) the significance of uptake into MDCK monolayers and (2) the relevance of binding capacity and affinity of RI-Tat-9 for the MDCK monolayer surface as it relates to our repulsion hypothesis that is described below. Figure 4 shows the time courses of the association at 1 μM tritiated RI-Tat-9 and 0 or 37 °C, with an acid wash. Acid wash is a common procedure for removing noninternalized surface-bound ligands without permeating the plasma membrane.[1,37]

The amount associated with MDCK monolayers at 0 °C is very small. Therefore, the result indicates that there is no significant uptake by the cell penetration mechanism, which is temperature-independent. Note, the association with MT2 cells at 0 °C is substantial, which is due to the high percentage of permeable dead cells in MT2 culture (~15% of the cells stained with trypan blue). The frangibility of MT2 cells is related to the way MT2 cells were made immortal.[38] Figure 4 also shows that the main difference between the two types of cells is the magnitude of the active uptake, defined by the difference between the 37 °C line and the 0 °C line in Figure 4 (replotted in Figure 5). At 60 min, the active uptake is 115.3 and 35.7 pmol/mg of protein for MT2 cells and MDCK monolayers, respectively, a 3.2-fold difference (Figure 5). The actual difference is likely to be greater because of the high percentage of dead cells in the MT2 cell culture. Therefore, to avoid this artifact the active uptake with HeLa cells is also included in Figure 5 (original data not shown). At 60 min, there is a 12.7-fold difference in the level of uptake between HeLa cells and MDCK monolayers. These comparisons indicate that there is not much active uptake into MDCK monolyaers either.

To further prove that there was no significant active uptake into MDCK monolayers, a comparison in cell energy-dependent uptake was made between MDCK monolayers and MT2 cells. Due to the frangibility of MT2 cells, the energy deprivation could not be extremely severe; i.e., it was done in the presence of glucose. Under this condition, a reduction in the measured level of cell association at 37 °C was seen only with MT2 cells, but not with MDCK monolayers in repeated experiments (Figure 6). The absence of an energy starvation effect on MDCK active uptake is consistent with the current observation of insignificant active uptake.

Since endocytosis was a likely mechanism underlying active uptake of RI-Tat-9, a panel of seven endocytosis inhibitors (chloroquine, nocodazole, calmidazolium, cytochalasin D, brefeldin A, nystatin, and filipin) affecting both the clathrin- and caveolae-mediated endocytosis were used to examine uptake into MDCK monolayers. No evidence for either endocytosis pathway was found (data not shown).

It has been demonstrated that peptides as large as 12 amino acids can be transported by some ABC family transporters (e.g., yeast α-matting factor by P-glycoprotein[39] and immunopeptides by TAP1/TAP2[40]). Since efflux transport might

(37) Haigler, H. T.; Maxfield, F. R.; Willingham, M. C.; Pastan, I. Dansylcadaverine inhibits internalization of ^{125}I-epidermal growth factor in Balb 3T3 cells. *J. Biol. Chem.* **1980**, *255*, 1239−1241.

(38) Harada, S.; Koyanagi, Y.; Yamamoto, N. Infection of HTLV-III/LAV in HTLV-1-carrying cells MT2 and MT4 and application on a plaque assay. *Science* **1985**, *229*, 563−566.

(39) Raymond, M.; Gros, P.; Whiteway, M.; Thomas, D. Y. Functional complementation of yeast ste6 by a mammalian multidrug resistance mdr gene. *Science* **1992**, *256*, 232−234.

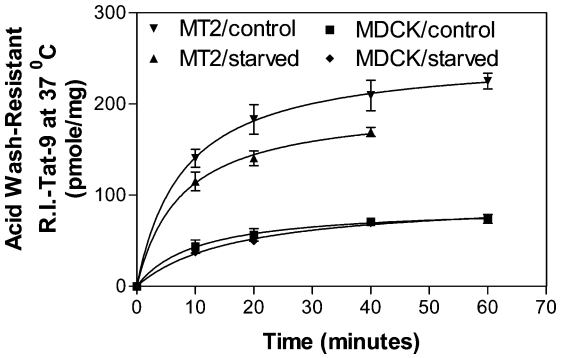

Figure 6. Effect of energy starvation on acid wash-resistant cell association at 37 °C. Energy starvation was achieved with a 30 min preincubation in the presence of 1% of sodium azide with MDCK or 20 min at 0.5% with MT2, followed by the incubation of the labeled peptide in the presence of a 10-fold excess of 2-deoxyglucose relative to glucose. The 60 min starved time point of MT2 is excluded since trypan blue staining showed an excess of cell death. Values are means of triplicate determinations ± the standard deviation. The R^2 of curve fitting by nonlinear regression was greater than 0.996.

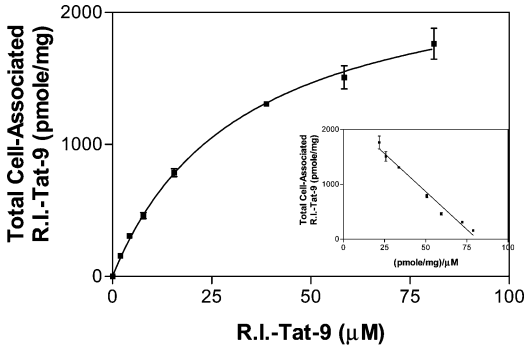

Figure 7. Concentration dependence of RI-Tat-9 association with MDCK monolayers at 60 min and 0 °C. MDCK monolayers grown on 24-well plates 2 days postconfluency were incubated with the indicated concentrations of tritiated RI-Tat-9 in incubation buffer at 0 °C for 60 min. The wells were then washed three times with ice-cold Hank's. The inset shows an Eadie−Hofstee plot of the same results. Values are means of triplicate determinations ± the standard deviation.

have obscured active uptake into MDCK monolayers, the possible involvement of ABC family transporters that are active in MDCK monolayers[35,36] was investigated. GF120918 (a P-glycoprotein-specific inhibitor) and MK571 (an inhibitor of the MRP family of transporters) were used. No significant effects by these inhibitors were found (data not shown).

To obtain the binding capacity and affinity of MDCK monolayers for the peptide, the concentration dependence was determined at 0 °C and 60 min, with no acid wash. The association at 0 °C without acid wash was constant from 10 min on (data not shown), indicating that the binding to the cell surface approached equilibrium after 10 min. Figure 7 shows that the equilibrium binding is not saturated up to 100 μM. A good fit using nonlinear regression and the equation for one-site binding [$Y = (B_{max}X)/(K_d + X)$] ($R^2 = 0.9985$) and a linear Eadie−Hofstee plot (Figure 7 inset) ($R^2 = 0.9791$) suggest one species of binding site on the surface of MDCK monolayers. The calculated B_{max} and K_d of the cell surface-binding site are 2416 ± 72 pmol/mg (or 1.7×10^8 sites per cell) and 32.5 ± 2.3 μM (mean ± standard deviation), respectively. The result indicates that the binding is of a high capacity and a low affinity, characteristic of nonspecific receptor binding.

Determination of RI-Tat-9 Permeability across Leaky Membranes and Leaky Cell Monolayers. The high-capacity, low-affinity binding of RI-Tat-9 to an MDCK monolayer suggested that repulsion of free RI-Tat-9 molecules by bound molecules might occur. A correlation was found (Table 2) that supported this hypothesis. At the end of a 3 h transport experiment, the ratio of the donor side to receiver side concentration across a leaky porous separation barrier appears to be a function of the amount bound to the barrier (R^2 of linear regression > 0.99). Three barriers were used: (1) Transwell inserts only, whose membrane was made of polycarbonate; (2) HeLa cell monolayers grown on Transwell inserts, whose membrane was made of polyester; and (3) Transwell inserts only, whose membrane was made of polyester. RI-Tat-9 was bound in an increasing amount in the order of the three barriers. The insert pore size of all three was 0.4 μm, or 400 nm. HeLa cells lack the ability to form tight junctions and therefore are leaky, although they grow into a monolayer on Transwell inserts.[41] The application of tritiated RI-Tat-9 to the donor side created a concentration difference across a barrier, which was enforced by subsequent samplings at the receiver side. At the end of experiment 1 in Table 2, the concentration difference was close to 1, or reached equilibrium, indicating that the amount of bound peptide was insufficient to retard the diffusion of the free peptide by repulsion. In experiments 2 and 3 in Table 2, the concentration differences were greater than 1, indicating that the bound amount was sufficiently high to retard the diffusion and/or to hold up a concentration difference by repulsion. At applied concentrations of 5.8 and 92 μM (Figure 7), an MDCK monolayer binds 17.3 and 98.7 pmol of RI-Tat-9/cm^2, respectively. As mentioned above, the data in Table 2 show a linear relationship between binding density and concentration difference across a leaky separation barrier (R^2 of linear regression > 0.99). Mathematically applying the two binding densities at MDCK monolayers to the linear regression equation from Table 2 yields 2.5- and 16-fold concentration differences, respectively. Therefore, it is inferred that the repulsion at the MDCK monolayer surface would be significant at ≥5 μM. Since the size of a modeled RI-Tat-9 molecule is 1.5 nm × 2.1 nm × 3.9 nm and the pore size of the filter is 400 nm, it is unlikely that RI-Tat-9

(40) Neefjes, J. J.; Momburg, F.; Hammerling, G. J. Selective and ATP-dependent translocation of peptides by the MHC-encoded transporter. *Nature* **1993**, *231*, 769−771.

(41) Spiryda, L. B.; Colman, D. R. Protein zero, a myelin IgCAM, induces physiologically operative tight junctions in nonadhesive carcinoma cells. *J. Neurosci. Res.* **1998**, *54*, 282−288.

Table 2. Correlation between the Amount of RI-Tat-9 Bound and the Concentration Difference across a Leaky Separation Barrier

experiment	leaky separation barrier	RI-Tat-9 bound (pmol/cm^2, mean ± standard deviation)	RI-Tat-9 concentration difference across the barrier (mean ± standard deviation)[a]
1	Transwell insert with polycarbonate membrane	8.0 ± 1.8	0.9 ± 0.1
2	HeLa monolayer grown on polyester insert membrane	50.1 ± 7.7	8.0 ± 0.8
3	Transwell insert with polyester membrane	110.5 ± 9.7	18.0 ± 2.5

[a] A fixed concentration (1 μM) of tritiated RI-Tat-9 was applied to the A side of an empty Transwell insert (pore size of 0.4 μm, area of 1 cm^2) or a HeLa cell monolayer grown on an insert. Frequent sampling was done at the B side as in a real A to B transport experiment. At the end of an experiment, the insert membranes or cell monolayers/membranes were washed three times and excised, and their radioactivities were determined along with A and B side buffers.

molecules are able to physically block transport. Therefore, it seems reasonable to speculate that repulsion occurs at the entrance and/or inside surface of a pore channel or a cell−cell gap.

Discussion

The ability to enhance macromolecular uptake into target cells is an important goal of modern drug delivery. While the use of Tat and other CPPs has become the focus of a significant number of investigations, many fundamental mechanistic questions have not been addressed and a number of conflicting reports have confused the interpretation and diminished the potential utility of this promising approach. On the basis of unpublished preliminary data and the cell penetration mechanism, we hypothesized that a highly positively charged Tat CPP would travel in tissues *in vivo* by diffusion over a distance until it was eliminated by means of binding to negatively charged macromolecules such as nucleic acids and proteoglycans. Diffusion could also be slowed or stopped by charge−charge repulsion resulting from the interaction between the free diffusing and bound Tat CPP molecules. Therefore, epithelial MDCK and Caco-2 cell monolayers were used in this study as model cell lines to quantitatively assess the cell penetration potential of a proteolysis-resistant Tat CPP (RI-Tat-9), using lymphocytic MT2 cells as a nonepithelial control. Caco-2 and MDCK cells were selected for study because of their wide use in evaluating the absorption potential of drugs and xenobiotics. However, it is recognized that the current studies need to be expanded to generalize the mechanisms to other ADME-related cell types (e.g., blood−brain barrier, liver, etc.) and pharmacological target cells (e.g., CD4$^+$ lymphocytes and macrophages, "cancerous" cells, etc.).

A retro−inverso form of Tat-9 (RI-Tat-9) was used in this study. "Retro" means that the amino acid sequence is reversed, while "inverso", also known as "inantio", indicates that each residue's chirality is inverted (D-form). A retro−inverso peptide theoretically presents side chains in an orientation very similar to that in the parent peptide[42] and can mimic the function of the parent peptide.[43,44] RI-Tat-9 was used in this study since the need for a proteolytically stable Tat CPP has been shown both *in vitro*[45] and *in vivo*,[26] an important consideration for drug delivery. Structure−function studies[9−12] have unequivocally demonstrated similar cell penetration capabilities for the L- and D-forms of a Tat CPP, as well as for an L-form and its RI-form that is very similar to ours (RI-Tat$_{48-57}$ in ref 12). We have also found that *in vitro*, RI-Tat-9 has potent anti-HIV-1 activity similar to that of the L-form (L. Wan, unpublished results). The fact that RI-Tat-9 and other labeled or conjugated L-forms of Tat CPPs[23,27] exhibit similar barrier behavior further validates the use of RI-Tat-9.

A significant finding of this study is that tritiated RI-Tat-9 increases mannitol permeability severalfold, suggesting that RI-Tat-9 modulates tight junction permeability. This finding is consistent with a confocal microscopic observation showing that fluorescein-labeled Cys-Tat$_{44-57}$ entered the paracellular space of MDCK monolayers, but was unable to cross either the apical or basolateral membranes.[27] In another more detailed study using rabbit nasal epithelium, polyarginine was shown to increase the paracellular permeability of hydrophilic molecules, a mechanism that appears to be common with other polycations.[46] Taken together, the cumulative data suggest that the enhanced, but still limited, paracellular passage of Tat is the predominant underlying mechanism for the observed *in vivo* organ or dermal penetration by Tat or polyarginine CPP fusion proteins or conjugates.[1−6,21,47,48]

Another significant finding in this study is that MDCK monolayers bind tritiated RI-Tat-9 with a high capacity and

(42) Goodman, M.; Chorev, M. On the concept of linear modified retropeptide structures. *Acc. Chem. Res.* **1979**, *12*, 1−7.

(43) Van Regenmortel, M. H.; Muller, S. D-Peptides as immunogens and diagnostic reagents. *Curr. Opin. Biotechnol.* **1998**, *9*, 377−382.

(44) Chorev, M.; Goodman, M. Recent developments in retro peptides and proteins: an ongoing topochemical exploration. *Trends Biotechnol.* **1995**, *13*, 438−445.

(45) Futaki, S.; Suzuki, T.; Ohashi, W.; Yagami, T.; Tanaka, S.; Ueda, K.; Sugiura, Y. Arginine-rich peptides. An abundant source of membrane-permeable peptides having potential as carriers for intracellular protein dlivery. *J. Biol. Chem.* **2001**, *276*, 5836−5840.

(46) Ohtake, K.; Maeno, T.; Ueda, H.; Natsume, H.; Morimoto, Y. Poly-L-arginine predominantly increases the paracellular permeability of hydrophilic macromolecules across rabbit nasal epithelium *in vitro*. *Pharm. Res.* **2003**, *20*, 153−160.

(47) Robbins, P. B.; Oliver, S. F.; Sheu, S. M.; Goodnough, J. B.; Wender, P.; Khavari, P. A. Peptide delivery to tissues via reversibly linked protein transduction sequences. *BioTechniques* **2002**, *33*, 190−194.

a low affinity. To our knowledge, this is the first quantitative nonspecific cell binding effect reported for a Tat CPP. There is apparently one species of binding site on a confluent MDCK monolayer at 1.7×10^8 sites per cell with a K_d of 32.5 μM. Remarkably, these values are close to those reported for the HeLa cell−Tat protein interaction ($>10^7$ sites/cell and saturation at ≥ 4 μM)[49] despite the differences in cells and ligands. Genetic and biochemical evidence indicates that highly negatively charged polysulfated proteaglycans are cell surface receptors for the Tat protein and a Tat CPP.[50,51] Proteaglycans are ubiquitously present on all animal cell surfaces, in basal lamina, and in connective tissues. They bind to a large number of soluble and insoluble ligands, performing a variety of functions.[52] Both Tat protein or Tat CPPs and cell surface proteaglycans are capable of high-affinity binding to other partners. Specific cell surface receptors for Tat protein or Tat peptides have a capacity of hundreds to thousands of sites per cell and a K_d in the nanomolar range,[53−56] while the K_d for specific binding of cell surface heparan sulfate proteaglycans to their ligands varies from 1 to 100 nM.[52] The drastically higher capacity and lower affinity of the interaction between RI-Tat-9 and a putative proteoglycan on MDCK monolayers suggest that the binding is nonspecific in nature, such as what occurs for a pure charge−charge type of interaction.

The last finding concerns the repulsion of free RI-Tat-9 molecules by molecules bound at the MDCK monolayer surface, an issue that is difficult to address. The correlation between the absolute amount of tritiated RI-Tat-9 bound to a leaky separation barrier and the peptide concentration difference across the barrier allows us to deduce that the repulsion would come into play at micromolar concentrations. Although the evidence is indirect, it permits the introduction of this novel mechanism for further investigation. The locations in the body where the repulsion may take place are where negative charge is concentrated, such as cell surface, cell nucleus, basal laminae underlying epithelia and endothelia, and connective tissue.

Combined, these results have important implications for Tat CPP-assisted drug delivery and the assessment of drug delivery potential using CPPs. It appears that oral and dermal delivery would be inefficient using these CPPs, due to the observed low permeability of epithelia and the deduced repulsion phenomenon. In the case of dermal delivery, millimolar concentrations of polyarginine conjugates had to be used,[47,48] further supporting our observations. For intravenous delivery, it would be of interest to know the behavior of endothelia toward Tat CPPs. Limited data suggest that the majority of endothelia that are nonfenestrated (i.e., except for those that are fenestrated, the endothelium of the kidney glomerulus, the sinusoidal endothelium of the liver and spleen, and the solid tumor microvessels) do exhibit limited permeability to Tat CPP.[25,26] On the other hand, Tat-assisted drug delivery would be feasible for blood cells and cells in the fenestrated reticulo-endothelial system (mainly in the liver and spleen). Lymphocytic cells, such as MT2 used in this study and Jurkat[32] cells, have been shown to actively take up Tat CPPs. In addition to the potential in assisting drug delivery, Tat CPP itself is being developed as an anti-HIV drug to target infected $CD4^+$ lymphocytes and macrophages, the latter being the main constituents of the reticulo-endothelial system.

There is little doubt that Tat CPPs promote the entry of a variety of cargos into cells and tissues, as evidenced by the functionality of these cargos. However, the mechanism of cell entry remains controversial.[6,33,57,58] The results of this study provide some interesting insights into the mechanisms of action of CPPs. Contrary to the reported cell penetration mechanism,[1−4] we found that MDCK monolayers exhibited minimal uptake, but MT-2 cells took up the peptide in a cell energy-dependent manner. However, while the cell type-specific difference could be explained by the lack of significant active uptake in MDCK cells, the underlying mechanism remains to be elucidated. Overall, these results add an additional weight to an emerging body of evidence[27−34,59−61] that disproves the cell type and cell energy independence of cell entry and favors endocytosis. Since

(48) Rothbard, J. B.; Garlington, S.; Lin, Q.; Kirschberg, T.; Kreider, E.; Leo McGrane, P.; Wender, P. A.; Khavari, P. A. Conjugation of arginine oligomers to cyclosporinA facilitates topical delivery and inhibition of inflammation. *Nat. Med.* **2000**, *6*, 1253−1257.

(49) Mann, D. A.; Frankel, A. D. Endocytosis and targeting of exogenous HIV-1 Tat protein. *EMBO J.* **1991**, *10*, 1733−1739.

(50) Tyagi, M.; Rusnati, M.; Presta, M.; Giacca, M. Internalization of HIV-1 Tat requires cell surface heparan sulfate proteoglycans. *J. Biol. Chem.* **2001**, *276*, 3254−3261.

(51) Sandgren, S.; Cheng, F.; Belting, M. Nuclear targeting of macromolecular polyanions by an HIV-Tat derived peptide. *J. Biol. Chem.* **2002**, *277*, 38877−38883.

(52) Bernfield, M.; Gotte, M.; Park, P. W.; Reizes, O.; Fitzgerald, M. L.; Lincecum, J.; Zako, M. Functions of cell surface heparan sulfate proteoglycans. *Annu. Rev. Biochem.* **1999**, *68*, 729−777.

(53) Denis, M. Tat protein from HIV-1 binds to *Mycobacterium avium* via a bacterial integrin. *J. Immunol.* **1994**, *153*, 2072−2081.

(54) Mitola, S.; Soaazni, S.; Luini, W.; Primo, L.; Borsatti, A.; Weich, H.; Bussolino, F. Tat-human immunodeficiency virus-1 induces human monocyte chemotaxis by activation of vascular endothelial growth factor receptor-1. *Blood* **1997**, *90*, 1365−1372.

(55) Albini, A.; Benelli, R.; Giunciuglio, D.; Cai, T.; Mariani, G.; Ferini, S.; Noonan, D. M. Identification of a novel domain of HIV Tat involved in monocyte chemotaxis. *J. Biol. Chem.* **1998**, *273*, 15895−15900.

(56) Scheidegger, P.; Weiglhofer, W.; Saurez, S.; Console, S.; Waltenberger, J.; Pepper, M. S.; Jaussi, R.; Ballmer-Hofer, K. Signaling properties of an HIV-encoded angiogenic peptide mimicking vascular endothelial growth factor activity. *Biochem. J.* **2001**, *353*, 569−578.

(57) Wright, L. R.; Rothbard, J. B.; Wendr, P. A. Guanidinium rich peptide transporters and drug delivery. *Curr. Protein Pept. Sci.* **2003**, *4*, 105−124.

(58) Zaro, J. L.; Shen, W.-C. Quantitative comparison of membrane transduction and endocytosis of oligopeptides. *Biochem. Biophys. Res. Commun.* **2003**, *307*, 241−247.

(59) Xia, H.; Mao, Q.; Davidson, B. L. The HIV Tat protein transduction domain improves the biodistribution of β-glucuronidase expressed from recombinant viral vectors. *Nat. Biotechnol.* **2001**, *19*, 640−664.

these results do not support the cell penetration mechanism defined by cell type and cell energy independence for MDCK and Caco-2 cells, the utility of these cell lines for evaluating drug delivery approaches using Tat CPPs is questionable. However, the use of Tat CPPs for enhancing macromolecular uptake into phagocytic cells (e.g., macrophages) and other important target cells appears to be promising. The general applicability of using CPPs across all cell types, the specific use of tat peptides, and the mechanism of action still require further study before these potentially important drug delivery agents can show their full potential.

Acknowledgment. This work was supported by NIH Grants AI 33789 and 51214. We thank Dr. J. W. Polli for GF120908 and Dr. Koch for MK561.

MP034014Y

(60) Console, S.; Marty, C.; Garcia-Echeverria, C.; Schwendener, R.; Ballmer-Hofer, K. Antennapedia and HIV transactivator of transcription (TAT) "protein transduction domains" promote endocytosis of high molecular weight cargo upon binding to cell surface glycosaminoglycans. *J. Biol. Chem.* **2003**, *278*, 35109−35114.

(61) Potocky, T. B.; Menon, A. K.; Gellman, S. H. Cytoplasmic and nuclear delivery of a TAT-derived peptide and a β-peptide after endocytic uptake into HeLa cells. *J. Biol. Chem.* **2003**, *278*, 50188−50194.